

HCN4 channels sense temperature and determine heart rate responses to heat

Yuejin Wu^{*1}, Qinchuan Wang¹, Jonathan Granger¹, Oscar Reyes Gaido¹, Eric Nunez Aguilar⁴, Andreas Ludwig², Anna Moroni³, Mario A. Bianchet⁴, Mark E. Anderson^{*1,5}

Supplementary Information

Supplementary Notes

Identification of amino acids important for heat sensing

From a thermodynamic point of view, the free-energy of channel activation by cAMP at pressure and volume constant ($\Delta G^{act.}$) is function of specific-heat at constant pressure (ΔC_p) of the cAMP-bound and apo (close) states and the temperature, described by equation 1:

$$\Delta G^{act.}(T) = \Delta G^{act.}(T_{ref}) + \Delta \Delta C_p^{act.} \left\{ (T - T_{ref}) - T \ln \left(\frac{T}{T_{ref}} \right) \right\} \quad [\text{eq. 1}],$$

where

$$\Delta \Delta C_p^{act.} = \Delta C_p^{cAMP-bound} - \Delta C_p^{apo} \quad [\text{eq. 2}]$$

The sign of $\Delta \Delta C_p^{act.}$ results in a convex (positive) or concave (negative) curvature of $\Delta G^{act.}(T)$, and its magnitude reflects the rate of change with the temperature [1]. A negative $\Delta \Delta C_p^{act.}$ will make $\Delta G^{act.}$ more negative (favorable) when the temperature increases (heat-sensitive) and a positive $\Delta \Delta C_p^{act.}$ has the opposite effect (cold-sensitive). A lower absolute value of the $\Delta \Delta C_p^{act.}$ diminishes the temperature dependence by decreasing the curvature of the $\Delta G^{act.}(T)$ as a function of the temperature.

The Q_{10} value is used to characterize the temperature dependence of the channel activation and is represented using the Arrhenius equations as a function of the energy barrier to overcome during the process ($\Delta E^\#$) [2] as:

$$Q_{10} = \exp \left(\frac{\Delta E^\#(T)}{k_B} \left(\frac{10}{T(T+10)} \right) \right) \quad [\text{eq. 3}],$$

where k_B is the Boltzmann constant, and T the measurement temperature in K. $\Delta E^\#$ is the free energy difference between the closed state (initial state) and the highest-energy intermediate (#) of the channel during the reaction path towards the cAMP activated state. At constant pressure and volume, $\Delta E^\#$ dependence on T is also described by an expression like equation 1:

$$\Delta E^\#(T) = \Delta E^\#(T_{ref}) + \Delta C_p^\# \left\{ (T - T_{ref}) - T \ln \left(\frac{T}{T_{ref}} \right) \right\} \quad [\text{eq. 4}],$$

Channel residues showing significant conformational changes during activation are expected to contribute to establishing the energy barrier that must overcome to become activated ($\Delta E^\#$).

Importantly, mutation of those residues may significantly affect the channel kinetics and temperature dependence.

To dissect the impact of such mutations on channel Q_{10} , we used the ratio between Q_{10} for mutant and wild type, combining equations 3 and 4. This resulted in:

$$\frac{Q_{10}^{Mut}(T)}{Q_{10}^{wt}(T)} = \exp \left\{ \left[\Delta\Delta E^{\#}(T_{ref}) + \Delta\Delta C_p^{\#mut-wt} \left((T - T_{ref}) - T \ln \left(\frac{T}{T_{ref}} \right) \right) \right] \left(\frac{10}{T(T+10)} \right) \right\} \text{ [eq. 5]},$$

where $\Delta\Delta E^{\#} = \Delta E^{\#mut}(T_{ref}) - \Delta E^{\#wt}(T_{ref})$ and $\Delta\Delta C_p^{\#} = \Delta C_p^{\#mut} - \Delta C_p^{\#wt}$, choosing an arbitrary T_{ref} . Mutations reducing the $\Delta E^{\#}$ with respect to that of the WT results in negative values of $\Delta\Delta E^{\#}$ decreasing the Q_{10} ratio, therefore reducing the mutant Q_{10} . Instead, positive values of $\Delta\Delta C_p^{\#}$ reduces the mutant Q_{10} , because of the negative T-explicit term that multiplies $\Delta\Delta C_p^{\#}$ in eq. 5.

In proteins, hydration of polar and apolar surfaces largely contribute with opposite signs to the ΔG of processes in which conformational changes are involved. Protein $\Delta C_p(T)$ are mostly proportional to the solvent-accessible surface area (SASA) of the protein [3]. Changes in the SASA between apo/closed and cAMP-activated states of the channel contribute to the differential change of both $\Delta E^{\#}$ and $\Delta C_p^{\#}$.

Strategically, by choosing mutations that minimize variations in the residue size, we can limit the structural changes in the mutated protein and neglect the otherwise larger energetic contributions by changing steric interactions when considering the free energy contributions. Mutation changing a residue's polar or apolar characteristics allows a heuristic estimate of the signs of $\Delta\Delta E^{\#}$ and $\Delta\Delta C_p^{\#}$ [1]. The $\Delta\Delta E^{\#}$ sign can be estimated considering the effects on the free energy of hydration of the initial, highest-energy, and final state of the mutation. The structure of the highest-energy intermediate is usually unknown, preventing direct calculation of $\Delta\Delta C_p^{\#}$. However, because of the strategy used to choose the mutations, the highest-energy intermediate will maximize the changes by exposure of apolar or sequestering (burying) of polar areas targeted in the mutation. Therefore, the sign of $\Delta\Delta C_p^{\#}$ matches the sign of the $\Delta\Delta C_p^{mut} = \Delta\Delta C_p^{act(mut)} - \Delta\Delta C_p^{act(wt)}$ that is calculated from known (or modeled) structures.

Heat sensing candidate residues

We calculated the $\Delta\Delta C_p^{mut}$ using models of the mutant structures based on the human channel structures (Supplementary Table 1).

M407Q. Met 407 exposes apolar area (81.0 \AA^2) during the activation, resulting in an unfavorable hydration enthalpy (Supplementary Fig. 5c). The exposure this apolar Met contributes positively to the energy of the high-energy intermediate. Mutating this Met to similar size residues, such as Gln, with a smaller apolar area and polar parts, will lower the energy barrier ($\Delta E^{\#}$) by increasing the energy of the initial state due to the unfavorable burying of its polar group and

decreasing the energy of the intermediate states by the favorable contribution of the solvation of polar parts of the residue. The resulting negative $\Delta\Delta E^\#$ and positive $\Delta\Delta C_p^\#$ (Supplementary Table 1) due to M407Q decreases the Q_{10}^{mut} .

Y409F. Tyr 409 buries 141.6 \AA^2 of SASA between its aromatic ring (76.2 \AA^2 of apolar area) and hydroxyl group (53.2 \AA^2 of polar area) during cAMP activation (Supplementary Fig. 5c). Y409F mutation eliminates the favorable enthalpy of hydration ($\Delta H < 0$) due to the polar area exposure in the apo/closed channel, and the unfavorable enthalpy of hydration of the burying of the tyrosine polar group during the activation. All these result in an increase of the initial state energy, and a potential reduction of the energy of intermediate states, resulting in an overall decrease of $\Delta E^\#$ (and a $\Delta\Delta E^\# < 0$). The negative sign $\Delta\Delta E^\#$ and the positive sign of $\Delta\Delta C_p^\#$ due to the mutation (Supplementary Table 1) also reduces the Q_{10}^{mut} .

F540Y. Phe 540 becomes solvent-exposed (54.9 \AA^2 , Supplementary Table 1) during activation, mostly apolar ($ASA_{apolar} = 33.1 \text{ \AA}^2$) with a large positive (unfavorable) contribution to the intermediates free- energy. The F540Y mutation buries in the initial state the tyrosine polar OH group adding a positive contribution to the free-energy of the initial state, and favorable hydration enthalpy during intermediate states to decrease the energy of the highest-energy intermediate. All the above results in negative $\Delta\Delta E^\#$ and positive $\Delta\Delta C_p^\#$ reducing the Q_{10}^{mut} . Interestingly, a tyrosine substitution is also observed in tardigrade.

K562M. The channel activation exposes 18.9 \AA^2 of the apolar area and buries 43.8 \AA^2 of the polar area of Lys 562 after activation, both having an unfavorable contribution that may contribute to the high of the energy barrier. Substitution with the more hydrophobic and shorter Met will decrease the unfavorable burying of the Lys polar NH_4 , resulting in a negative $\Delta\Delta E^\#$, however, the large negative $\Delta\Delta C_p^\#$ may negate partially or totally reverse the effect of $\Delta\Delta E^\#$.

F613Y. Similarly, to Phe 540, Phe 613 becomes solvent-exposed during activation (44.4 \AA^2 , Supplementary Table 1). Also, in this case, a substitution with a tyrosine residue will add a polar group to be exposed with a favorable contribution. However, our homology model of the mutant showed that the additional OH group becomes relatively buried, only exposing a small amount of polar area (3.6 \AA^2) resulting in a small negative $\Delta\Delta C_p^{mut-wt}$ (Supplementary Table 1) that may attenuate the effect of $\Delta\Delta E^\#$ in the Q_{10}^{mut} .

Interspecies considerations for modelling

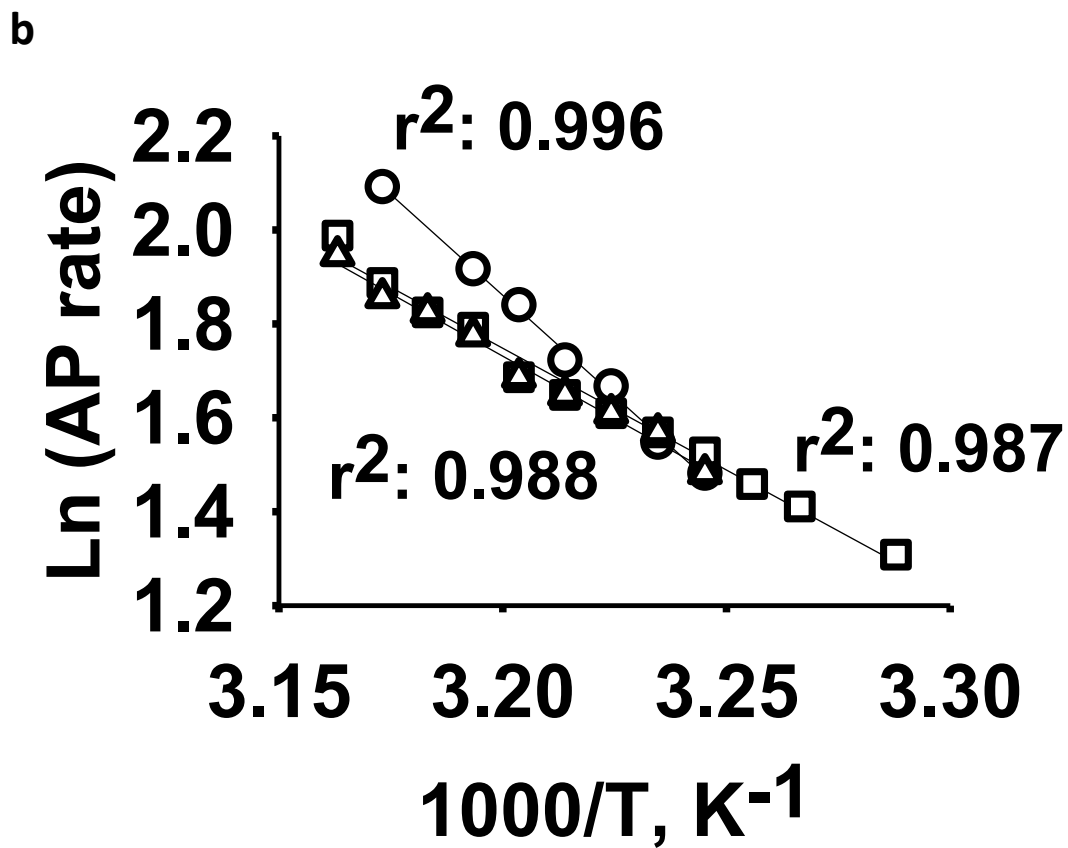
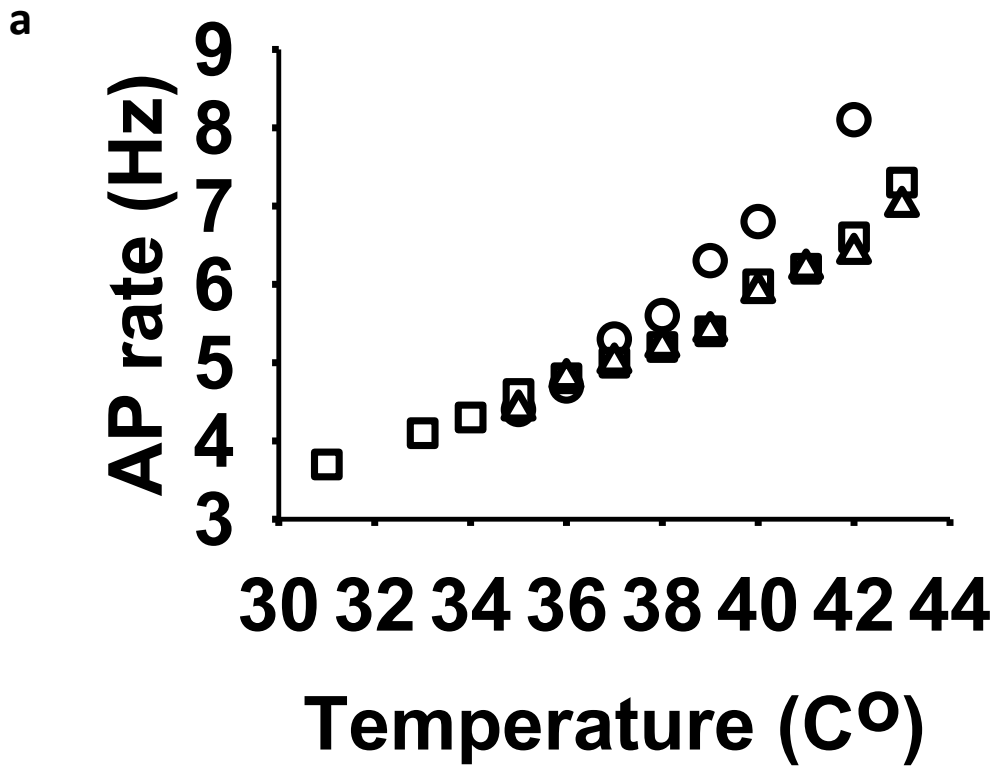
All HCN4 human (6GYN and 6GYO) and rabbit structures display hydrophobic and hydrophilic interactions of lipids in the S4-linker-S5 region, which may have critical structural functions [4]. Both human and rabbit-activated structures are similar. However, in the human HCN4, the S4-linker-S5 region in the apo/closed state is farther away from the activated state than the apo rabbit structures. The rabbit protein preparations of the Saponaro et al. structural determination[4] used different detergent lipid mixtures to stabilize the rabbit apo cAMP in an open conformation, showing the S4-linker-S5 region conformation closer to the activated state,

which is similar in both species. This suggest that the linker region presents the largest changes during activation, and we focused our analysis of these changes using human apo and cAMP activated structures.

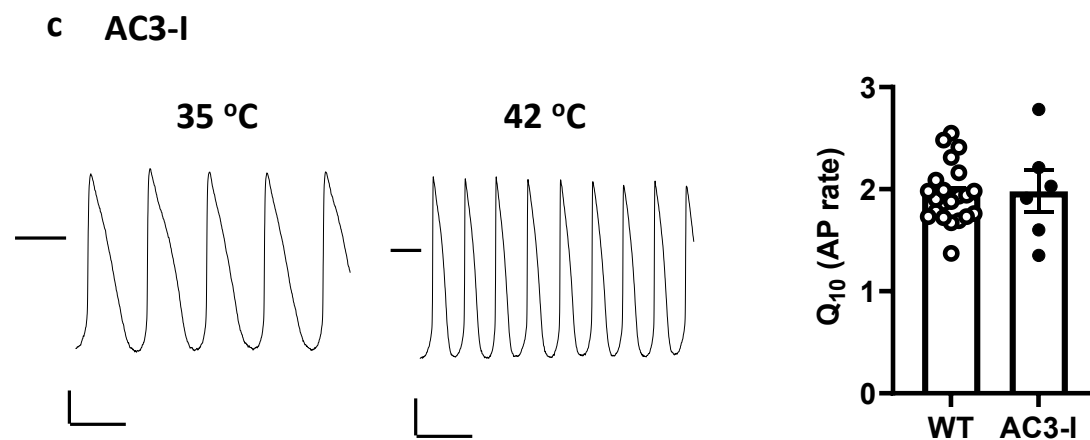
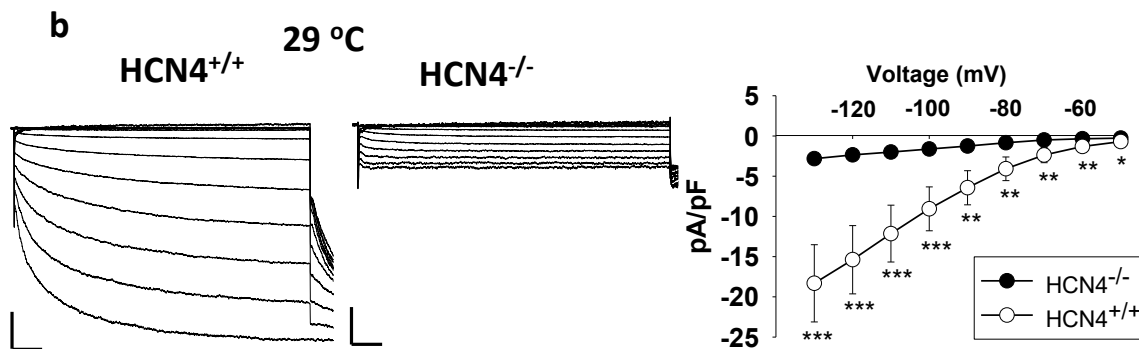
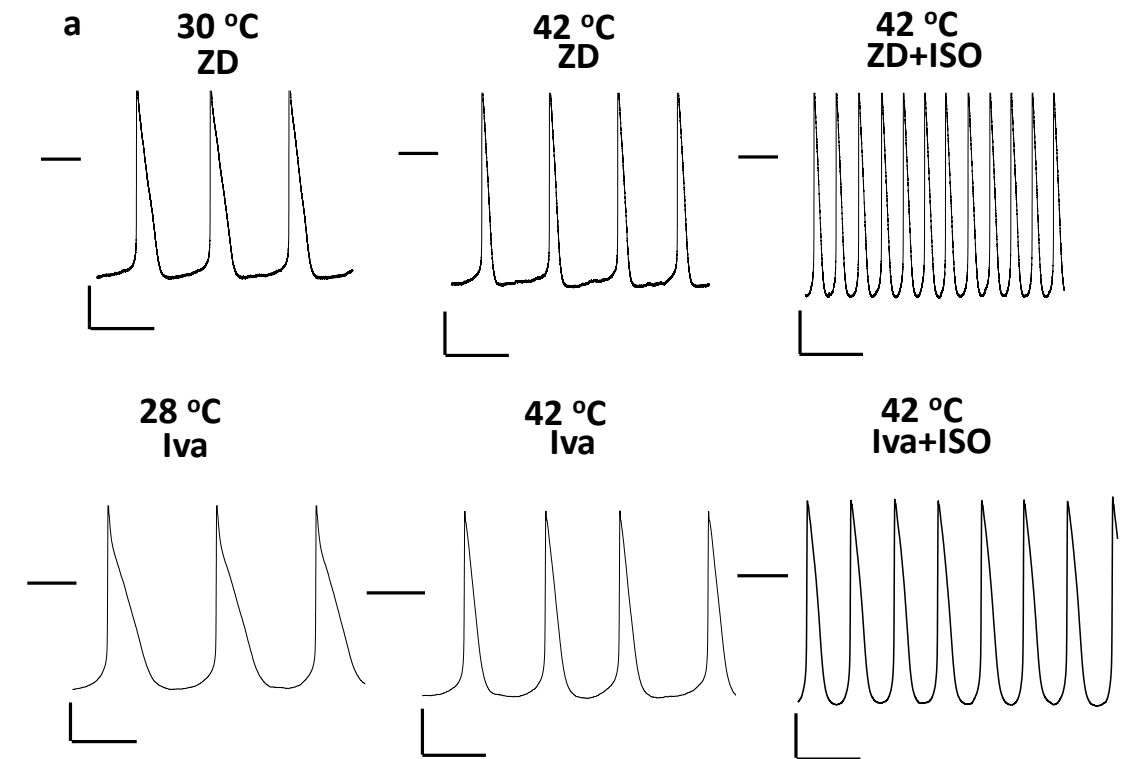
Supplementary References

1. Chowdhury, S., B.W. Jarecki, and B. Chanda, *A molecular framework for temperature-dependent gating of ion channels*. Cell, 2014. **158**(5): p. 1148-1158.
2. Sterratt, D.C., *Q10: The Effect of Temperature on Ion Channel Kinetics*, in *Encyclopedia of Computational Neuroscience*, D. Jaeger and R. Jung, Editors. 2013, Springer New York: New York, NY. p. 1-3.
3. Makhatadze, G.I. and P.L. Privalov, *Heat capacity of proteins: I. Partial molar heat capacity of individual amino acid residues in aqueous solution: Hydration effect*. Journal of Molecular Biology, 1990. **213**(2): p. 375-384.
4. Saponaro, A., et al., *Gating movements and ion permeation in HCN4 pacemaker channels*. Mol Cell, 2021. **81**(14): p. 2929-2943 e6.

Supplementary Figures



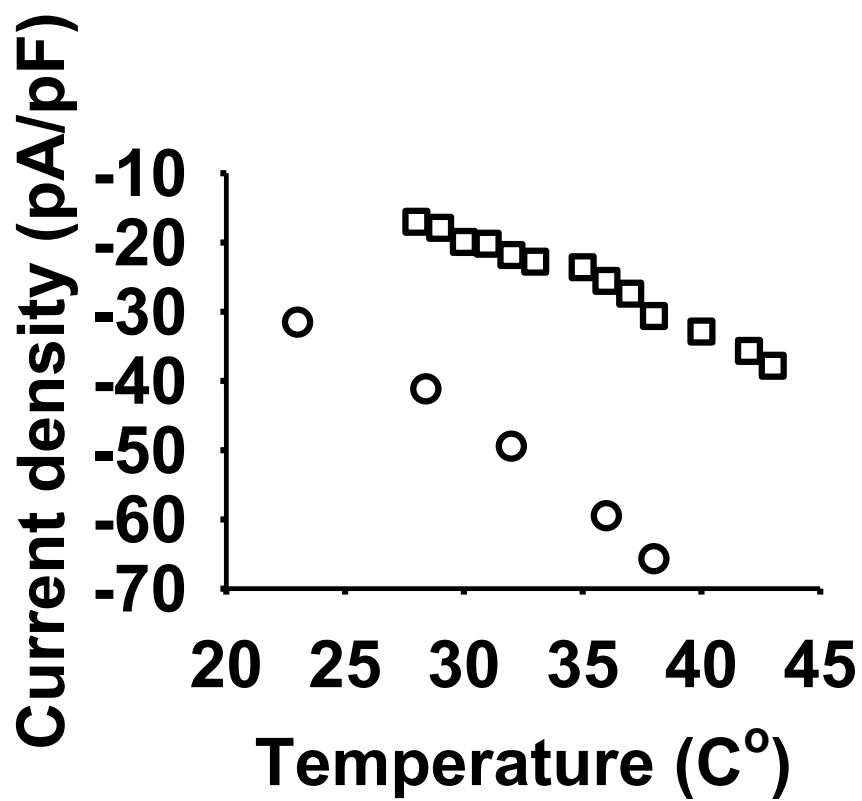
Supplementary Fig 1. The Arrhenius plot of action potential rate increase with temperature a, examples of action potential (AP) rate increase with temperature from 3 SAN cells (symbols circle, square, and triangle represent different cells). **b,** The Arrhenius plots of the data from the same cells in the **a**., the line and r^2 are from linear regression.



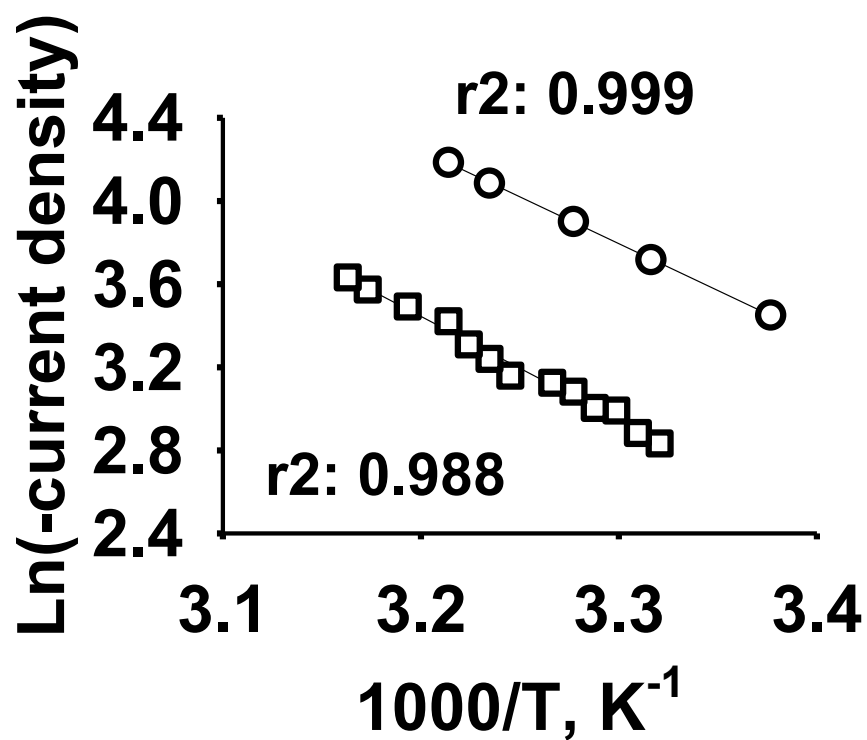
Supplementary Fig 2. Spontaneous action potentials and *Hcn4* gene deletion in SAN cells

a, Representative spontaneous action potential recordings from isolated mouse SAN cells. ZD7288 (ZD, 4 μ M, upper panels), and Ivabradine (Iva, 4 μ M, lower panels), reduced temperature-dependent, but not ISO (isoproterenol, 1 μ M) dependent action potential rate increases. Example tracings and summary data are calculated by comparing the same cell under two or more conditions in all panels. **b**, Representative I_f currents recorded from cultured *Hcn4* floxed (left panel) and cultured *Hcn4* floxed SAN cells co-incubated with Cre recombinase expressing adenovirus (middle panel). Summary data for current-voltage relationships (right panels) from control (left panel, n=6) and *Hcn4* excised SAN cells (middle panel, n=8). Analysis using Student's *t*-test and Mann-Whitney Rank Sum Test as appropriate. * $p < 0.05$, ** $p < 0.01$, *** $p < 0.001$. **c**, Representative action potentials recorded from the same SAN cell with transgenic expression of AC3-I, a CaMKII inhibitory peptide at lower (left) and higher (middle) temperatures. Summary Q_{10} data for spontaneous action potential rates are shown on the right. Data are presented as mean \pm SEM, n=22, WT, n=6, AC3-I.

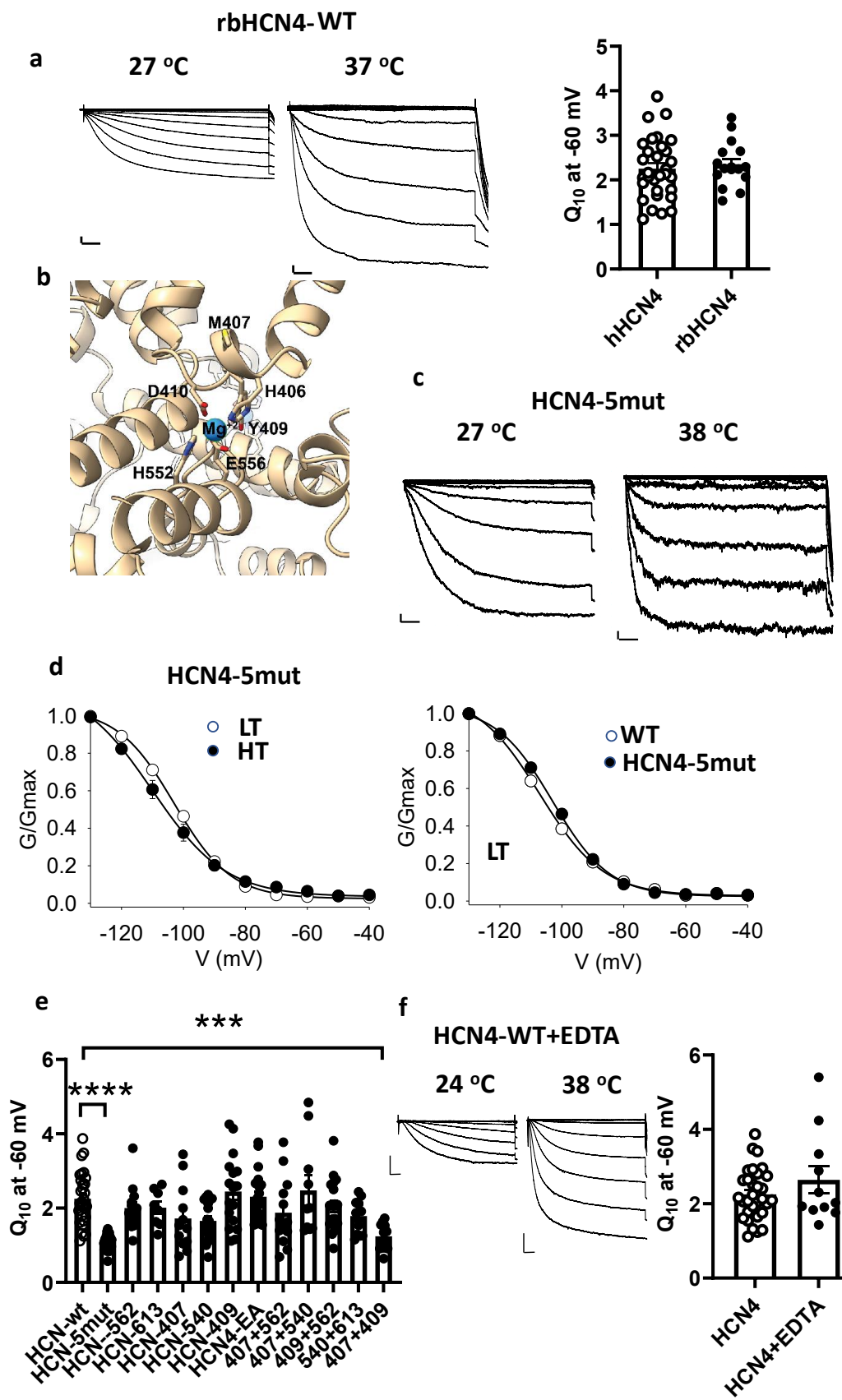
a



b



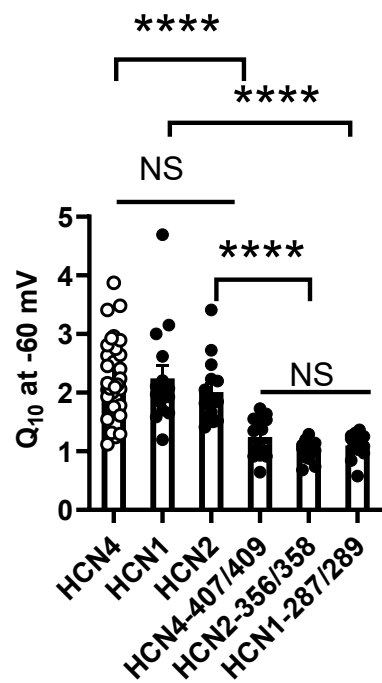
Supplementary Fig 3. The Arrhenius plot of I_f current or HCN4 current increase with temperature **a**, An example of I_f current density at -110 mV from a single SAN cell (symbol square) and HCN4 current density from a HEK cell expressing HCN4 channels (symbol circle) increasing with temperature. **b**, The Arrhenius plots of the data from the same cells in **a**, the line and r^2 are from linear regression.



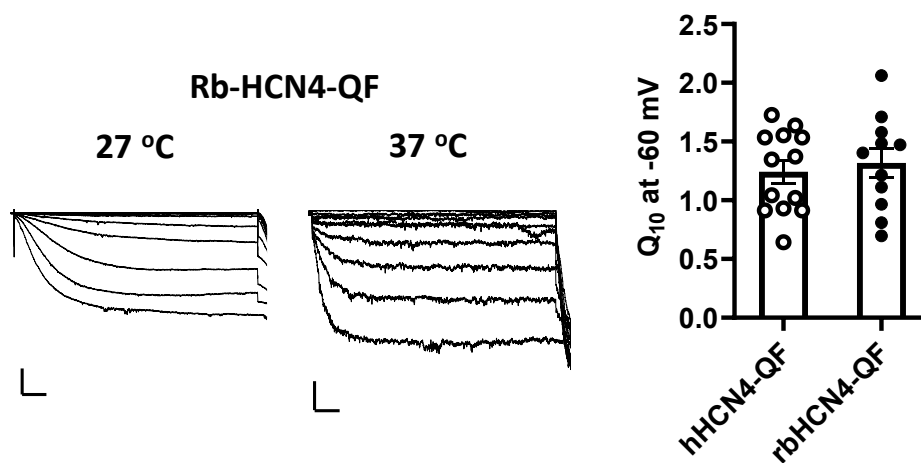
Supplementary Fig 4. Structural and functional analysis of HCN4 heat resistant mutants

a, HCN4 channel currents recorded at lower (left) and higher (middle) temperature from HEK cell expressing rbHCN4-WT (rabbit WT HCN4) channels. Summary data of Q_{10} at -60 mV from hHCN4 WT compare to rbHCN4 WT (right). Data are presented as mean \pm SEM n=31, hHCN4, n=16, rbHCN4. Example tracings and summary data calculated by comparisons using the same cell in all panels. **b**, Structural representation of key sites on the S4-S5 intracellular linker and Mg^{2+} coordination sites for the cAMP-activated structure of HCN4 (6GYO), (see Methods). **c**, Representative current traces recorded from a HEK cell expressing HCN4-5mut (see Methods) under low (left) and high (right) temperatures. **d**, Mean activation Boltzmann fits recorded from HCN4-5mut channels under low (LT) and high (HT) temperatures (left panel, n=45, LT (low temperature range 25-29°C) and n=22, HT (high temperature range 35-41°C) or (right panel) from WT (n=20, LT (low temperature range 25-29°C)) and HCN4-5mut channels (n=45, LT (low temperature range 25-29°C)). **e**, Summary Q_{10} data for HCN4 current recorded at -60 mV from various HCN4 WT and mutant channels (see Methods and Table S2). One way ANOVA test, ***p<0.001, ****p<0.0001. Data are presented as mean \pm SEM n=31, HCN4, n=29, 5mut, n=13, HCN4-562, n=8, HCN4-613, n=12, HCN4-407, n=18, HCN4-540, n=17, HCN4-409, n=22 HCN4-EA, n=13, 407+562, n=10, 407+540, n=19, 409+562, n=12, 504+613, n=13, 407+409. **f**, Representative HCN4 currents recorded with 10 mM EDTA in the pipette solution under low and high temperatures (left and middle panel). Summary Q_{10} data are shown on the right panel for normal (n=31) and EDTA (n=11) pipette solutions. Data are presented as mean \pm SEM.

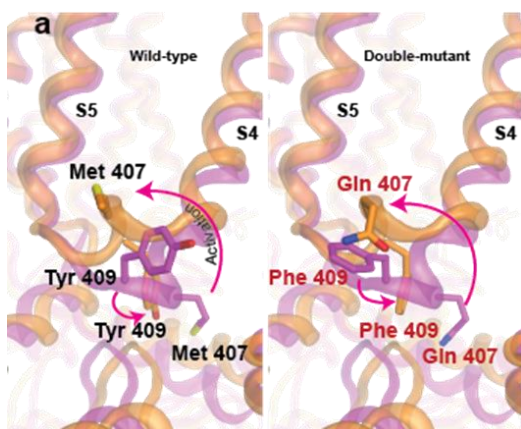
a



b



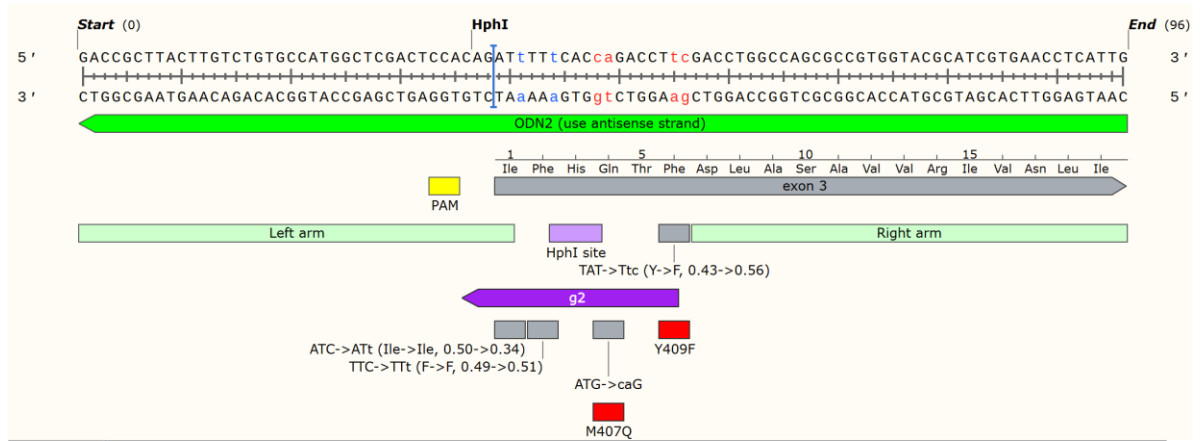
c



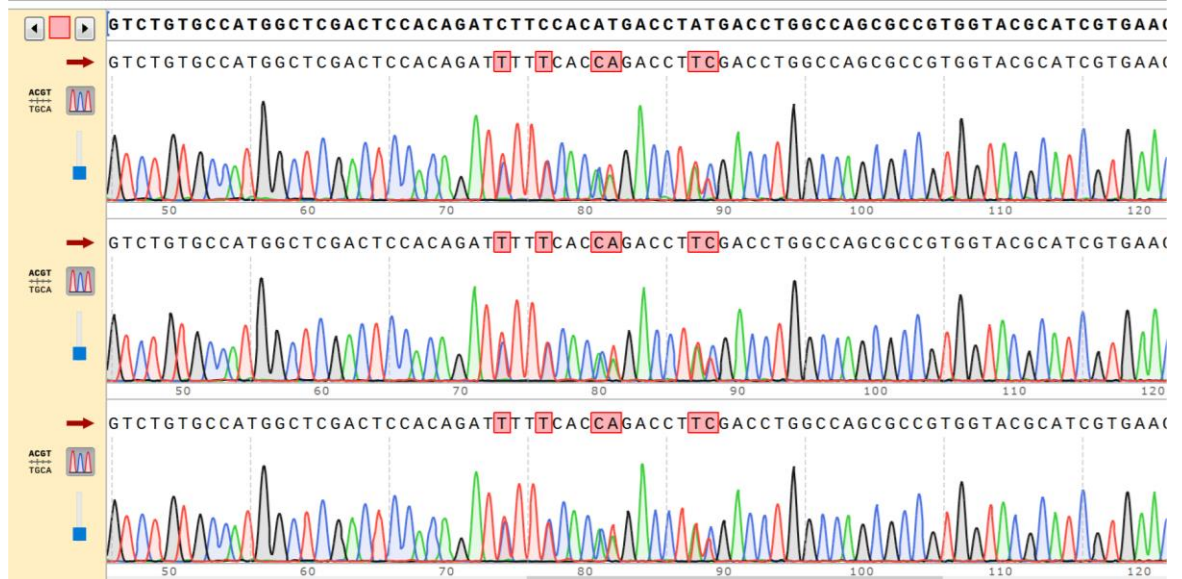
Supplementary Fig 5. Similar HCN channel family responses to heat

a, Q_{10} summary data for I_f recorded at -60 mV from HEK 293 cells expressing WT and heat insensitive mutant HCN1, 2 and 4. One-way ANOVA test, NS, not significant, **** $p < 0.0001$. Data are presented as mean \pm SEM $n=31$, HCN4, $n=15$, HCN1, $n=15$, HCN2, $n=13$, 407/409, $n=14$, 356/358, $n=18$, 287/289. **b**, I_f currents recorded at lower (left) and higher (middle) temperature from HEK cell expressing rabbit rbHCN4-M408Q/Y410F channels. Summary data of Q_{10} at -60 mV from human hHCN4 mutant compared to rbHCN4 mutant on the right. Summary data calculations were made using the same cell exposed to high and low temperatures in panels **a** and **b**. Data are presented as mean \pm SEM, $n=13$, hHCN4-QF, $n=11$, rbHCN4-QF. **c**, S4-S5 intracellular linker in the closed and cAMP activated structure. Model of WT Met 407 and Tyr 409 in the closed (magenta) and activated (orange) conformations (left panel). Model of the M407Q and Y409F mutants in closed (magenta) and activated (orange) conformations. The residue rotamers were chosen by a rotational search algorithm by the program MOE. Figures were drawn using MOE (see Methods).

a

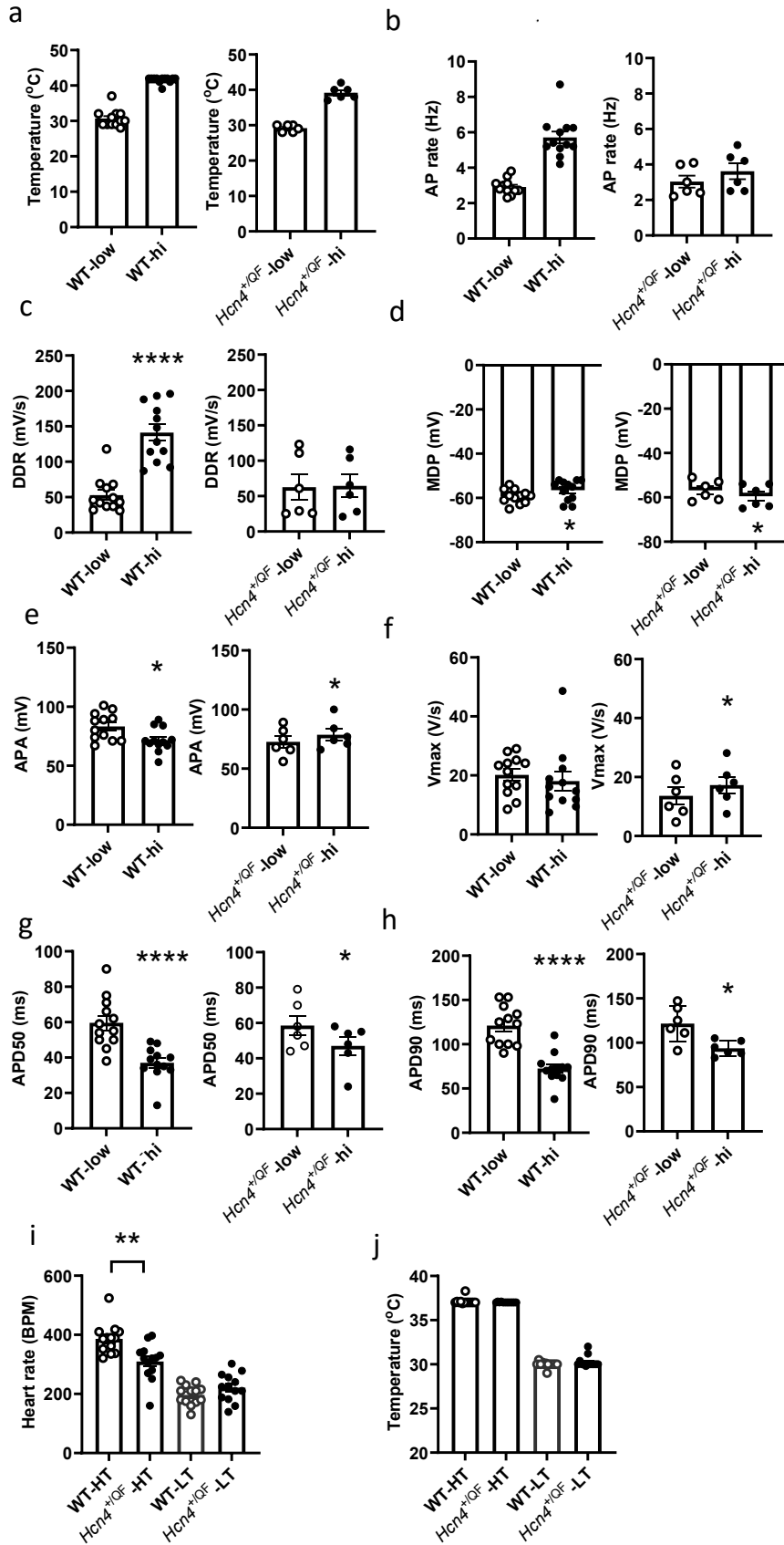


b



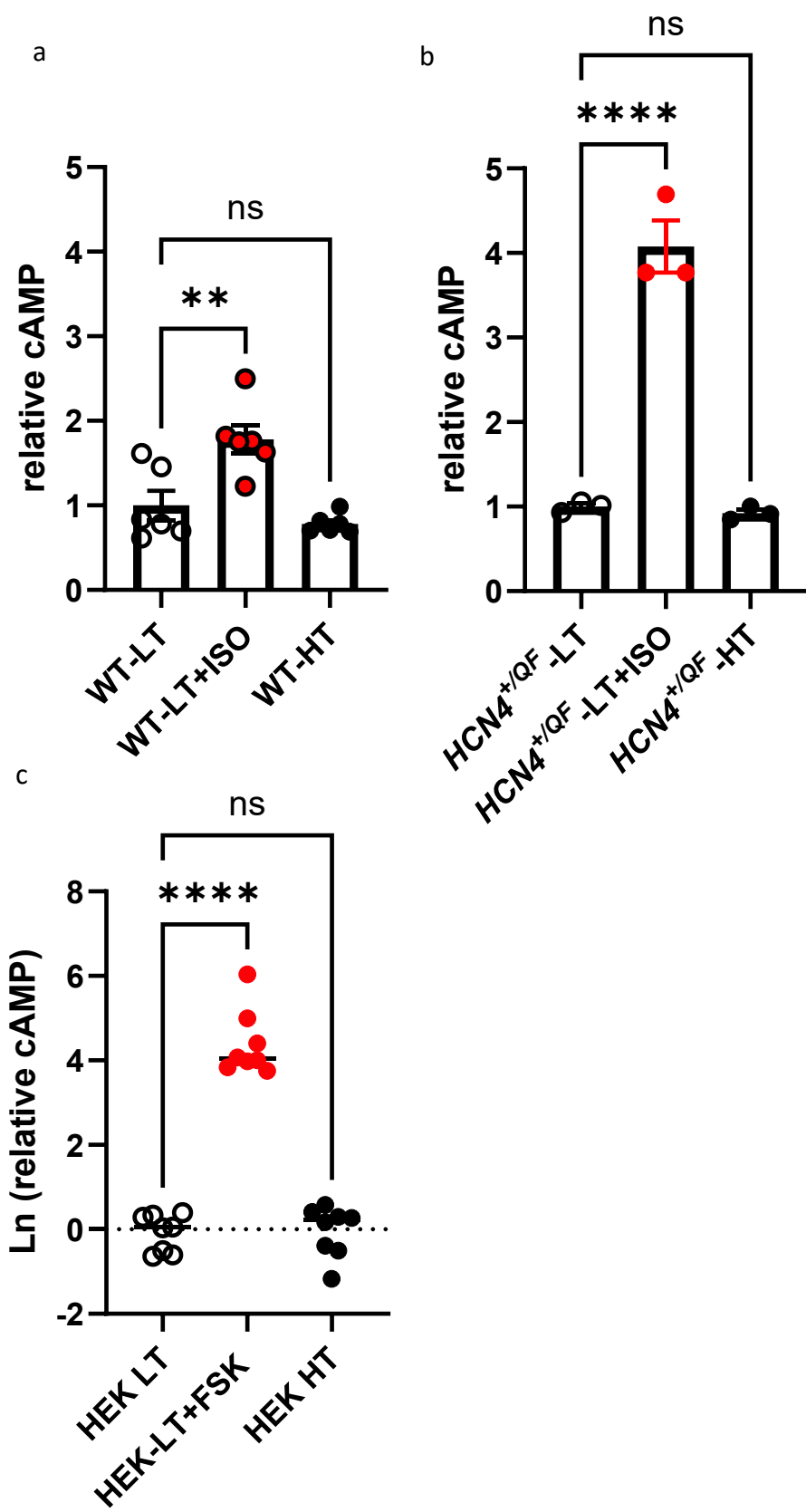
Supplementary Fig 6. Mouse *Hcn4* CRISPR strategy

a, The DNA sequence shows the CRISPR-modified *Hcn4* genomic region. Silent mutations are shown in blue and missense mutations in red. The location of CRISPR guide (g2) binding site, PAM, HphI restriction site, and codons for M407Q and Y409F are indicated. For the silent mutations introduced to the codons for Ile404 and F405, the codon usage frequencies of the original and modified codons are indicated in parentheses. **b**, Sanger sequencing chromatograms of three successfully targeted founder mice.



Supplementary Fig 7. Action potential parameters

All AP parameters are from single SAN cells isolated from heterozygous *Hcn4*^{+/^{QF}} and WT littermate control mice (**a-h**). All data from a-j are presented as mean \pm SEM, the raw data and n numbers for all the data presented in this figure see the source file. **a**, Temperature range of high temperature (HT) and low temperature (LT) for the AP recordings. **b**, AP rate (Hz). **c**, diastolic depolarization rate (DDR). **d**, maximal diastolic potential (MDP). WT, *p=0.019, *Hcn4*^{+/^{QF}}, *p=0.014, paired Student's *t* test (two tailed). **e**, Action potential Amplitude (APA). WT, *p=0.016, *Hcn4*^{+/^{QF}}, *p=0.012, paired Student's *t* test (two tailed). **f**, Maximal rising slope (Vmax). *Hcn4*^{+/^{QF}}, *p=0.037, paired Student's *t* test (two tailed). **g**, APD50 (AP duration at 50% repolarization). WT, ****p=0.0001, *Hcn4*^{+/^{QF}}, *p=0.028, paired Student's *t* test (two tailed). **h**, APD90 (AP duration at 90% repolarization). WT, ****p=0.0001, *Hcn4*^{+/^{QF}}, *p=0.029, paired Student's *t* test (two tailed). **i-j**, Summary of ex vivo heart rates and temperatures from heterozygous *Hcn4*^{+/^{QF}} mice compared to their littermate WT controls. **i**, heart rate in beats/min (BPM) and **j**, shows the temperatures recorded in the immersion bath (see Methods) for high (HT) and low temperatures (LT). The heart rate and temperature data are calculated in all panels by comparing the same hearts. ** p=0.0015 by one way ANOVA.



Supplementary Fig 8. cAMP level in isolated SAN cells and HEK 293 cells

a, Relative cAMP level measured from isolated SAN cells from WT control mice under different treatments as indicated. **b**, Relative cAMP level measured from isolated SAN cells from heterozygous *Hcn4*^{+/^{QF}} mice under different treatments as indicated. **c**, Relative cAMP level measured from HEK 293 cells under different treatments as indicated. Statistical analysis performed using one way ANOVA followed by the Sidak's multiple comparisons test. **p<0.01, ***p<0.0001. HT, higher temperature; LT, lower temperatures; ISO, isoproterenol; FSK, forskolin. (See Methods for more details).

Supplementary Tables

Supplementary Table 1. Δ SASA, and $\Delta\Delta C_p^{\text{activation}}$ of residues showing a change in solvent exposure during activation. . The Jupyter notebook of a python worksheet calculations mutant models and dataset used are deposited in Zenodo (DOIs: 10.5281/zenodo.14635261 and 10.5281/zenodo.14635412)

Amino acid	Δ SASA (all) [\AA^2]	ΔC_p^{act} [$\text{J K}^{-1} \text{mol}^{-1}$]	Mut.	$\Delta\Delta C_p^{\text{Mut}}$ [$\text{J K}^{-1} \text{mol}^{-1}$]
Met 407	111.9	69.5	M407Q	11.4
Phe 540	54.9	33.5	F540Y	23.2
Lys 562	-21.7	103.3	K562M	-84.4
Phe 613	44.4	40.7	F613Y	-7.2
Tyr 409	-141.6	-141.6	Y409F	77.8
Ile 661	-99.2	-202.9	—	—
Arg 668	-57.8	12.0	—	—
Glu 695	-83.5	-22.9	—	—

Supplementary Table 2. Activation curve parameters

	$V_{1/2}$ (mV) \pm SEM control	K (mV) \pm SEM control	n	$V_{1/2}$ (mV) \pm SEM +cAMP	K (mV) \pm SEM +cAMP	n	cAMP-induced $V_{1/2}$ shift \pm SEM	Temp-induced $V_{1/2}$ shift \pm SEM
HCN4 wt (LT)	-107.3 \pm 0.7	10.4 \pm 0.7	20	-96.1 \pm 1.2	14.1 \pm 1.3	14	11.2 \pm 1.4***	
HCN4 wt (HT)	-96.0 \pm 1.4###	10.5 \pm 0.8	21	-91.1 \pm 2.8	11.1 \pm 1.2	13	4.9 \pm 3.1	11.3 \pm 1.6***
HCN4 M407Q-Y409F (LT)	-105.3 \pm 1.2	8.9 \pm 0.4	27	-104.6 \pm 1.6	9.1 \pm 1.3	13	0.7 \pm 2.0	
HCN4 M407Q-Y409F (HT)	-108 \pm 1.5	10.7 \pm 0.8	13	-103.2 \pm 2.3	8.4 \pm 0.9	10	4.8 \pm 2.7	-2.7 \pm 1.9
HCN4 M407Q-Y409F-F540Y-K562M-F613Y (LT)	-102.7 \pm 1	8.3 \pm 0.3	45					
HCN4 M407Q-Y409F-F540Y-K562M-F613Y (HT)	-108.2 \pm 2	9.9 \pm 0.7	22					-5.5 \pm 2.2**
HCN4 R669E-T670A (LT)	-105.2 \pm 1.5	11.5 \pm 0.8	22	-107.3 \pm 1.9	11.1 \pm 0.8	11	-2.1 \pm 2.4	
HCN4 R669E-T670A (HT)	-97.9 \pm 1.6###	10.7 \pm 1.0	18	-102.0 \pm 3.7	9.0 \pm 1.3	7	-4.1 \pm 4.0	7.3 \pm 2.2**
HCN4 Y527F-R669E-T670A (LT)	-95.9 \pm 1.5###	11.4 \pm 0.6	12	-98.6 \pm 1.2	11.1 \pm 0.6	13	-2.7 \pm 1.9	
HCN4 Y527F-R669E-T670A (HT)	-96.3 \pm 1.9###	9.9 \pm 1	9	-97.2 \pm 2.8	12.2 \pm 0.9	5	-0.9 \pm 3.4	-0.4 \pm 2.4
HCN4 wt with EDTA (LT)	-101.4 \pm 1.6	13.7 \pm 0.7	13					
HCN4 wt with EDTA (HT)	-95 \pm 1.4###	12 \pm 0.8	12					6.4 \pm 2.1**
HCN1 wt (LT)	-84.9 \pm 1.6	9.1 \pm 0.6	16	-84.3 \pm 4.6	13.7 \pm 3.9	3	0.6 \pm 4.9	
HCN1 wt (HT)	-91.2 \pm 1.8#	11.1 \pm 0.9	15	-83.3 \pm 3.9	9.8 \pm 1.4	3	7.9 \pm 4.3	-6.3 \pm 2.4*
HCN1 M287Q-Y289F (LT)	-96.7 \pm 2.7###	12.4 \pm 0.8	9					
HCN1 M287Q-Y289F (HT)	-100.0 \pm 2.9###	12.0 \pm 0.6	6					-3.3 \pm 4.0
HCN2 wt (LT)	-97.4 \pm 1.5	10.0 \pm 0.6	32	-90.0 \pm 1.9	9.6 \pm 0.7	16	7.4 \pm 2.4**	
HCN2 wt (HT)	-87.2 \pm 2.5###	9.6 \pm 0.9	18	-81.0 \pm 2.8	10.2 \pm 0.9	10	6.2 \pm 3.7	10.2 \pm 2.9***
HCN2 M356Q-Y358F (LT)	-107.9 \pm 1.3###	9.9 \pm 0.9	19	-107.3 \pm 0.8	9.1 \pm 0.7	16	0.6 \pm 1.5	

HCN2 M356Q-Y358F (HT)	-107.0±2.5 ^{###}	14.0±1.2	12	-108.0±3.5	13.0±1.5	8	-1.0±4.3	0.9±2.8
HCN2 R618E-T619A (LT)	-102.8±1.2 ^{##}	8.7±0.4	25	-103.4±0.9	8.8±0.4	22	-0.6±1.5	
HCN2 R618E-T619A (HT)	-104.7±1.0 ^{##}	9.9±0.8	16	-101.7±1.9	9.4±0.7	15	3±2.1	-1.9±1.6

Half-activation voltage ($V_{1/2}$) and inverse slope factor (k) obtained by fitting data to a Boltzmann function (see Methods) in absence or presence of cAMP (1 mM); LT (Low temperature, 22-29 °C) and HT (High temperature, 35-43 °C); n=number of cells tested in each condition.
^{###}p<0.001, ^{##}p=0.009 (HCN2 R618E-T619A (LT)) and p=0.009 (HCN2 R618E-T619A (HT)), [#]p=0.017 (HCN1 wt (HT)) by One-way ANOVA with Multiple Comparisons versus Control Group (Holm-Sidak method) compared to wt HCN4, HCN1 or HCN2 at LT; ^{***}p<0.001, ^{**}p=0.005 (HCN2 wt(LT)), p=0.006 (HCN4 wt with EDTA (HT)), p=0.002 (HCN\$ R669E-T670A (HT)), p=0.008 (HCN4 M407Q-Y409F-F540Y-K562M-F613Y (HT)), ^{*}p=0.014(HCN1 wt(HT)) by Student’s *t*-test (two-tailed) compared to control condition (cAMP compare with without cAMP or HT condition compare with LT condition).